Scientific paper

Identification of Novel HPPD/PPO Dual-Target Inhibitors Through Virtual Screening of Multiple Pharmacophore Models

Pan-Xiu Zhang¹, Juan Shi¹, Ying Fu^{1,2,*}

¹ Department of Chemistry, College of Arts and Sciences, Northeast Agricultural University, Harbin 150030, China

² Key Laboratory of Agricultural Functional Molecule Design and Utilization of Heilongjiang Province, Harbin 150030, China

* Corresponding author: E-mail: fuying@neau.edu.cn

Received: 02-03-2025

Abstract

The development and identification of dual target herbicides was one of primary approach to addressing the issue of weed resistance. Protoporphyrinogen oxidase (PPO) and p-hydroxyphenylpyruvate dioxygenase (HPPD) are two important targets of photosynthesis in plants. Different from the traditional single target drug design, this study focuses on HPPD and PPO dual target drug design. Hiphop pharmacophore models of HPPD and PPO targets were constructed use commercial pesticides, and CBP pharmacophore models were constructed based on protein complexes. Over millions of molecules were screened using pharmacophore models and 8 compounds were obtained. Candidate compounds chelated with Fe(II) in HPPD and formed stable π - π interactions with key residues in HPPD active pocket. Most compounds produced hydrogen bond interactions and π - π interactions with residues in PPO. Combined with a multiple visual screen process, potential compounds with dual-target inhibition effect were obtained.

Keywords: Dual target herbicide, Target-based drug design, HPPD, PPO, Virtual screening

1. Introduction

Weeds are a major hazard to crops, competing with them for sunlight, water and nutrients in the soil. ^{1,2} As an economical, efficient, and reliable solution for weed control, herbicide application is key role to ensuring high and stable crop yields. The continuous application of herbicides led the weed resistance increasing, and the impact of herbicide residues on crops and the environment. There is an urgent need to develop of safety, low-impact, low toxicity and highly efficient novel herbicides. ^{3,4}

During plant photosynthesis, the action sites of pigment synthesis are tetrapyrrole, carotenoid and plastoquinone. As shown in Figure 1, the synergistic effect of three enzymes, protoporphyrinogen oxidase (PPO) phytoene desaturase (PDS) and p-hydroxyphenylpyruvate dioxygenase (HPPD) in plants were illustrated.⁵ In the process of chlorophyll synthesis, PPO is the key catalytic enzyme in the process of tetrapyrrole biosynthesis. PPO catalyzes protoporphyrinogen IX to produce protoporphyrin IX in plants under the oxygen and sunlight conditions.^{6,7} Protoporphyrin IX chelates with metal ions in chloroplasts to

produce chlorophyll.^{8–10} Protoporphyrinogen IX is unable to bind to the active site of PPO after being treated with PPO inhibitors in the presence of light and oxygen, protoporphyrinogen IX is accumulated in cytoplasm and converted to photosensitive protoporphyrin IX, causing the cell to rupture and the plant death. 11-13 In addition to chlorophyll, carotenoids, acting as light-harvesting pigments in photosynthetic reaction, protect photosynthesis from chlorophyll triplet and singlet oxygen damage. 14 PDS is a rate-limiting enzyme in carotenoid synthesis and catalyzes the symmetric desaturation of phytoene to carotenoid. 15,16 Inhibition of PDS causes the phytoene accumulation in plants, disrupting carotenoid and chlorophyll synthesis and ultimately resulting in weeds death.¹⁷ In plants, HPPD is an important oxidoreductase involved in the tyrosine metabolic pathway, catalyzing the conversion of p-hydroxyphenylpyruvate (HPPA) to homogentisic acid (HGA), which further reacts to produce plastoquinone and tocopherol. 18-20 Plastoquinone is the key cofactor of PDS. HPPD inhibitors hinder the synthesis of plastoquinone and tocopherol, 21,22 and the synthesis of carotenoid is indirectly affected by the decrease of the content of plas-

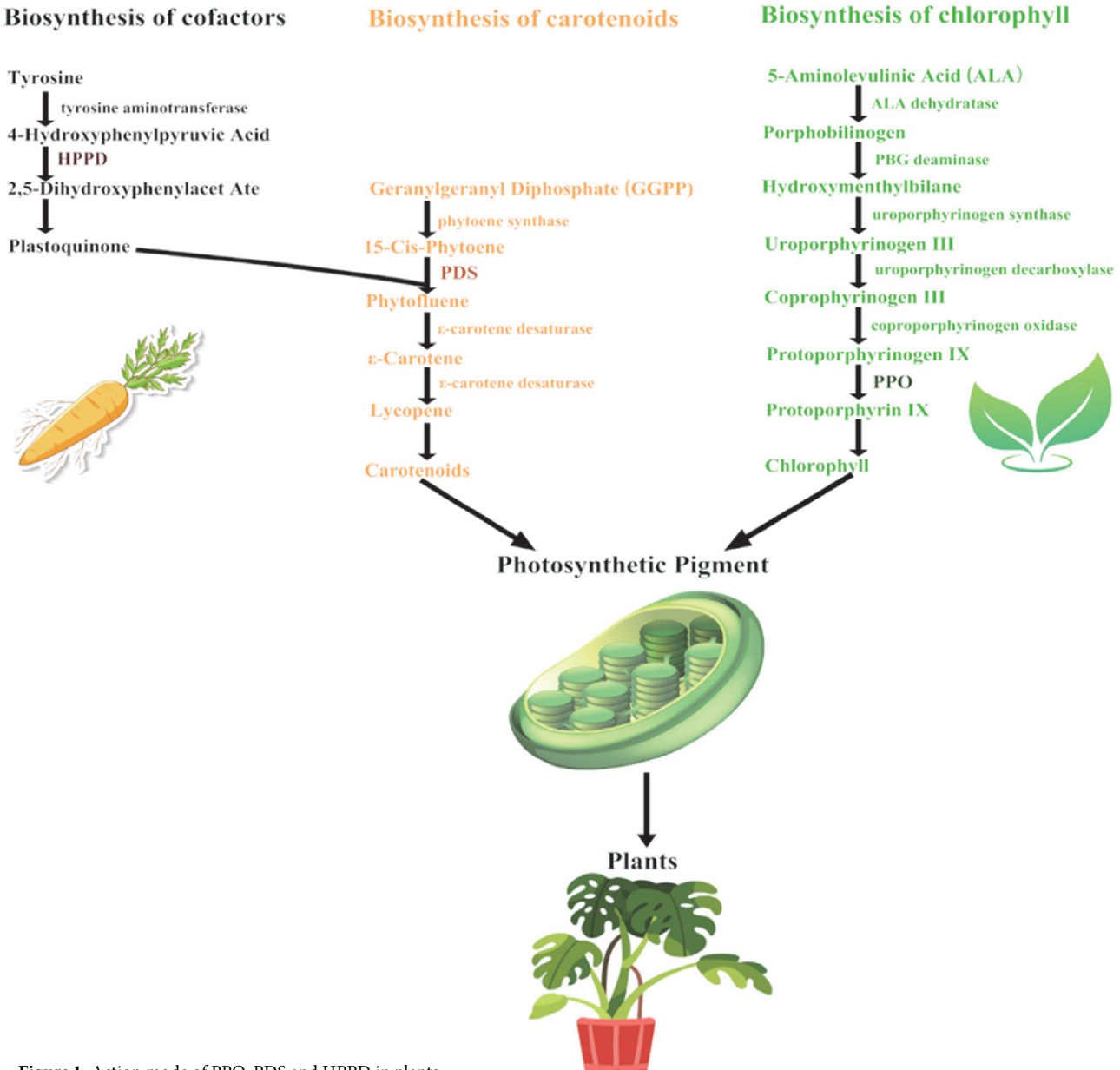


Figure 1. Action mode of PPO, PDS and HPPD in plants.

toquinone, eventually leaf bleaching of the plant leaves.^{23,} The results show that leaves albinism occurred when HPPD and PPO inhibitors are applied, further affecting weed growth by reducing the content of chlorophyll.

Compared with traditional single-target drug design, multi-target drug acts on multiple targets in the same body at the same time, producing synergistic effects on each target.²⁵ If a certain target is mutated, the drug will maintain therapeutic efficacy by inhibiting other targets, and avoiding drug resistance caused by single-target mutations. Sorafenib is a multi-target drug that has been marketed for the treatment of cancer by acting on metallothionein 1G(MT1G), DNA methyltransferase 1 (NMT1), Krüpple-like Factor 4(KLF4), and Carbonic anhydrase 9(CA9) in hepatocellular carcinoma.²⁶ Virtual screening

of the dual FMS-like tyrosine kinase 3 (FLT3) and mitogen-activated protein kinase (MAPK)-interacting kinases 2 (MNK2) inhibitor in the treatment of acute myeloid leukemia was conducted by molecular docking methods and cell experiments, the results showed that the obtained candidate K783-0308 exhibited inhibitory effect for the target FLT3 and MNK2.²⁷ Novel dual-target of HPPD and PDS inhibitors were screened using pharmacophore models, molecular docking and structure optimization.⁵

Pharmacophore models are collections of spatial and electronic features, in continuous of our study on multi-target albino herbicides, HPPD and PPO multi-target pharmacophore models were constructed and 1024513 small molecules were screened. Pharmacophore models based on common characteristics of molecules (Hiphop)

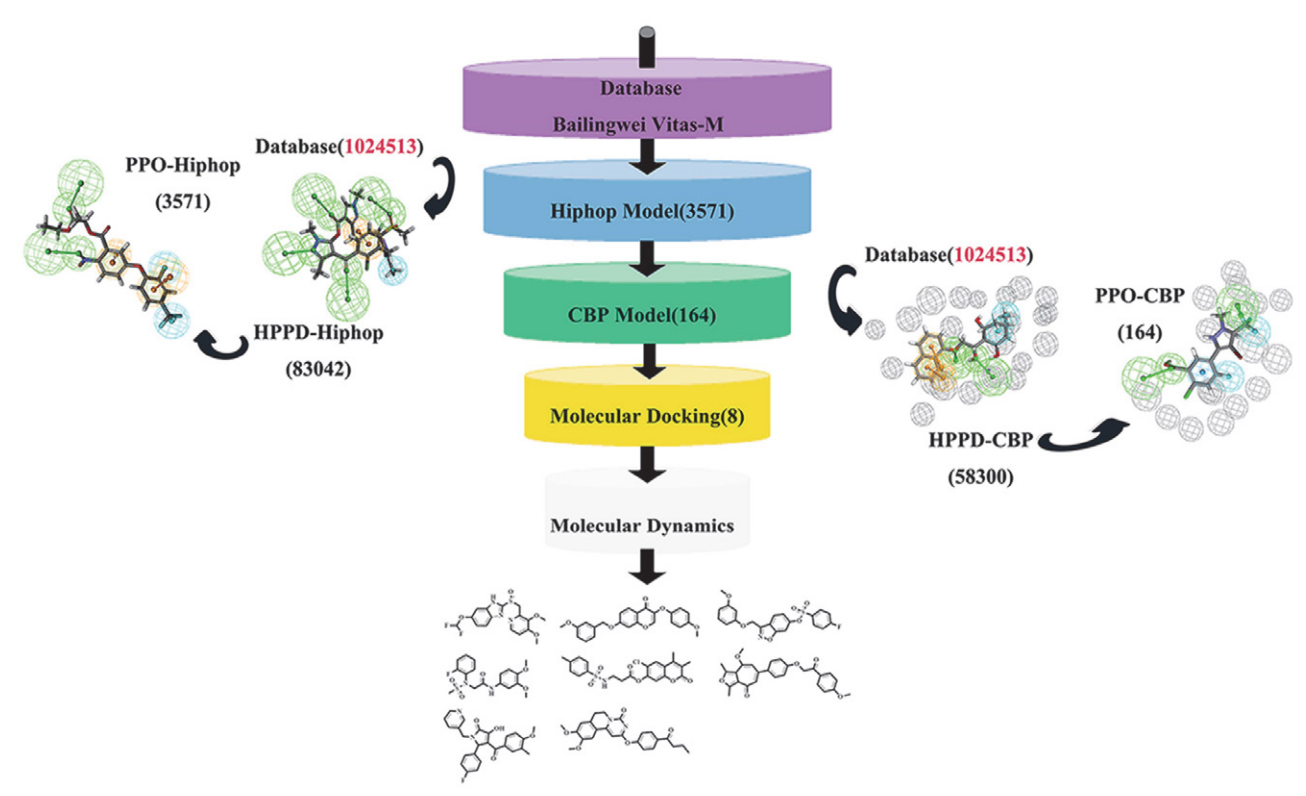


Figure 2. The workflow of multi virtual screening base on dual herbicide target.

and complex-based pharmacophore models (CBP) were constructed respectively, molecular docking and molecular dynamics (MD) simulation were performed on candidate compounds. Finally, 8 potential compounds with inhibitory effects on HPPD and PPO were obtained. The workflow of virtual screening based on the pharmacophore model is shown in Figure 2.

2. Experimental

2. 1. Database Collection and Preparation

1024513 Compounds were extracted from Bailingwei and Vitas-M (https://vitasmlab.biz) databases, and screened according the Lipinski rules compounds. Compounds were conformational optimized with Discovery Studio (DS, Biovia Inc. San Diego, CA, USA, 2020), the 3D database was built with the "Build 3D Database" module, the conformation number was set to 200, and the BEST method was selected for conformation generation.

2. 2. Generation and Verification of Hiphop Pharmacophore Model and Virtual Screening

The Hiphop pharmacophore was established in "Common Feature Pharmacophore Generation model of DS. According to the common characteristics of active compounds, pharmacophore models were generated based on the overlap of these common characteristics and

subsequently applied to virtual screening. Regarding HP-PD, six commercial HPPD herbicides topramezone, pyrasulfotole, cypyrafluone, tolpyralate, fenpyrazone and tripyrasulfone were collected as the training set to construct HPPD-Hiphop pharmacophore models, the physicochemical properties are listed in Table S1. All ligands were set the MaxOmitFeat feature with 0 and Principal feature with 2. Compound feature elements were selected using the "Edit and Cluster Features" tool. The characteristic elements of hydrogen bond donor (HBD), hydrogen bond acceptor (HBA), aromatic ring (AR) and hydrophobic (HY) were selected to produce pharmacophore. Hiphop pharmacophore was constructed using the "Common Feature Pharmacophore Generation" function in the "Create Pharmacophores Automatically" module. The BEST was selected to produce 10 pharmacophore and 200 conformations with a cut-off value of 10 kcal·mol⁻¹. To test the reliability of the pharmacophore model, the compounds reported in literature on HPPD inhibitors and structures that have no effect on HPPD were collected. 16 Active compounds and 10 inactive compounds (Figure S1) were collected as a testing set, the "Search, Screen and Profile" module was used to evaluate the constructed Hiphop pharmacophore match with the test set. Input File Pharmacophores were loaded, and 10 pharmacophore models were input. The Maximum Conformation number was set to 200 and the Energy Threshold was set to 10.

In the same way as the construction process of the pharmacophore model of HPPD, 6 commercial PPO herbicides fluroximin, fomesafen, fluoroglycofen, lactofen, acif-

luorfen and ethhoxyfen-ethyl were used as the training set to construct the PPO-Hiphop pharmacophore model, the physicochemical properties of six commercial PPO inhibitors were shown in Table S2. The PPO pharmacophore construction and validation were the same as that for HPPD pharmacophore model. The PPO testing set consisted of 13 active compounds and 12 inactive compounds (Figure S2).

HPPD-Hiphop pharmacophore model was used to screen the 3D database, and the remaining compounds were screened by PPO-Hiphop pharmacophore model.

2. 3. Generation and Verification of CBP Pharmacophore Model and Virtual Screening

Different from the Hiphop model, the construction of the CBP model was based on single receptor-ligand crystal complex interaction, the number of training set was fixed. To ensure the accuracy of the constructed CBP model, a diverse set of active and inactive compounds must be collected for rigorous validation. Arabidopsis thaliana HPPD (AtHPPD) (PDB ID: 7X5Y) (resolution $1.50 \text{ Å})^{19}$ and crystalline small compound were defined as receptor and ligand, and the "Interaction Pharmacophore Generation" module of DS was used to generate a CBP pharmacophore model. Through a literature search, 47 Active compounds and 68 inactive compounds were collected to validate the CBP pharmacophore model (Figure S3). Validation was set to True, Active Ligands were set to All, Inactive Ligands were set to All and other parameters were set to default. Commercial HPPD inhibitors included triketone and pyrazole structure, and the active compounds in the validation set were mainly composed of these two structures. To examine the relationship between the collected active compounds and inactive compounds, principal component analysis (PCA) was employed to analyze the chemical space. The molecular weight, number of hydrogen bond donors and receptors, number of rotatable bonds and log p descriptors of the collected compounds were used as input value.²⁸

The PPO-CBP pharmacophore model was constructed using the same protocol as for HPPD. Nicotiana tabacum PPO (*Nt*PPO, PDB ID: 1SEZ, resolution 2.90 Å)²⁹ was selected to establish the CBP pharmacophore model. The validation set of the PPO pharmacophore model consisted of 19 active compounds and 43 inactive compounds (Figure S4). The active compounds were dominated by diphenyl ether structures.

2. 4. Molecular Docking

In order to ensure the accuracy of molecular docking results, complex structures of plant origin with resolution less than 2.0 Å were selected for study. Mesotrione and oxyfluofen were used as positive controls, the AtHPPD (PDB ID: 1TFZ) (resolution 1.8 Å)³⁰ and NtPPO crystal structure

were downloaded from the PDB database for molecular docking with compounds. Sequence information for 1TFZ and 1SEZ is provided in Table S3. Proteins and ligands were treated with DS and SYBYL-X 2.0. The unnecessary water molecules and side chains of the Protein were removed, the Protein was treated with "Prepare Protein" under the "Molecular" module in DS, the lost residues were supplemented, and the position of the protein was added with the CHARMm force field. 5,31,32 The Sketch module in SYBYL-X 2.0 was used to process compounds. Under the Tripos force field, Gasteiger-Huckel charge was used to optimize the molecules, the maximum iteration coefficient was selected as 1000, and the energy convergence was 0.005 kcal mol⁻¹.

CDOCKER in DS "Receptor-Ligand Interactions" module was used for molecular docking. The high temperature dynamic rotation method was used to generate the random ligand configuration, and then the lattice based simulated annealing algorithm was used to optimize the ligand configuration, using the "From Current Selection" under the "Define and Edit Binding Site" module to define the binding site of the protein around the ligand. The binding site size was set to 10Å, other settings were default.³³ The AtHPPD binding site information was x: 45.937, y: 38.936, z: 51.499, and the *Nt*PPO binding site information was x: -39.832, y: -6.094, z: 28.669. Set the Dock Ligands (CDOCKER) parameter to define the coordinates and radius of the docking site, and adjust the Pose Cluster Radius parameter to 0.5 to maximize diversity in the docking conformations. After docking, the interactions between ligands and proteins were analyzed and the top 10 conformational combinations with higher -CDOCKER ENERGY values were preserved.

2. 5. MD Simulation

MD simulation was commonly used to aid in the study of dynamic atomic details, reveal the dynamics of receptor-ligand interactions and explain the molecular mechanisms behind them, allowing for a more accurate and convenient assessment of the binding affinity of selected compounds.^{34–36} In order to verify the stability of binding between the screening results and proteins, MD simulation was further tested by using Desmond module of Schrodinger software. Biological macromolecules mostly used the water model, after the structure of the complex was optimized, the system was constructed by a simple point charge (SPC) water model and the ligand-protein complex was placed in a regular hexahedral box filled with water molecules. 37-39 To ensure the simulation system was neutral, appropriate counterbalance ion neutralization was added. With the parameters set under the Molecular Dynamics module, the complex was simulated for 100 ns at 298 K temperature and 1.01 bar pressure. In addition, the maximum interaction was set to 2000, the convergence threshold was set to 1.0 kcal mol⁻¹ A⁻¹, and the OPLS_2005 force field was used to minimize the energy of the complex system.⁴⁰ The steepest descent and limited memory Broyden Fletcher Goldfarb Shanno algorithm minimize system energy with 5000 steps until it reached the gradient threshold of 25 kcal mol⁻¹ Å⁻¹. Mesotrione and oxyfluofen were used as positive control groups in MD simulation. After the simulation, RMSD of protein skeleton, residues around ligands and binding pockets, and ligand heavy atoms were analyzed for the equilibrium state and stability of the complex. RMSD of the backbone was the main index to evaluate the stability of the system.

The Desmond module of Schrödinger software was selected to calculate the molecular mechanics/generalized born surface area (MM/GBSA) for the compounds, the binding free energy (ΔG_{bind}) was divided into molecular mechanical terms and solvation energy, respectively, reflecting the degree of binding between compounds and proteins.^{41, 42}

3. Results and Discussion

3. 1. Hiphop Pharmacophore for Virtual Screening

All of the ten pharmacophore models generated according to the HPPD training set had six characteristic elements and ranked above 85, which proved the reliability of the pharmacophore models, as shown in Table 1. By matching the HPPD-Hiphop pharmacophore models with the training set, the hydrogen bond receptors were nearby the oxygen and nitrogen atoms of the training set, the aromatic ring center was formed at the benzene ring, and the

hydrophobic characteristics could be found at the methyl of the compounds (Figure S5). To ensure the accuracy of the pharmacophore models, the Hiphop pharmacophore models were verified through the testing set (Figure 3(a)). The pharmacophore models could well recognize the active and inactive compounds, and HPPD-Hiphop pharmacophore models-02, 03 and 05 were more effective than other models. The Hiphop pharmacophore model-02 had a score of 89.143, was selected for further screening (Figure 3(b)). The pharmacophore signature elements included 1 aromatic ring center, 1 hydrophobic feature, and 4 hydrogen bond receptors.

Table 1 Result parameters of HPPD-Hiphop pharmacophore model.

Num-	Features	Rank	Direct	Partial	Max
ber			Hit	Hit	Fit
01	RHAAAA	91.10	111111	000000	6
02	RHAAAA	89.14	111111	000000	6
03	RHAAAA	89.14	111111	000000	6
04	RHAAAA	88.67	111111	000000	6
05	RHAAAA	88.42	111111	000000	6
06	RHAAAA	88.26	111111	000000	6
07	RHAAAA	88.25	111111	000000	6
08	RHAAAA	87.84	111111	000000	6
09	RHAAAA	87.84	111111	000000	6
10	RHAAAA	87.83	111111	000000	6

Rank: Indicates the fit values of the pharmacophore.

Direct Hit: indicates the match between the pharmacophore and the training set molecule.

Partial Hit: indicates the number of pharmacophore features that match the training set molecule.

Max Fit: indicates the matching of pharmacophore features.

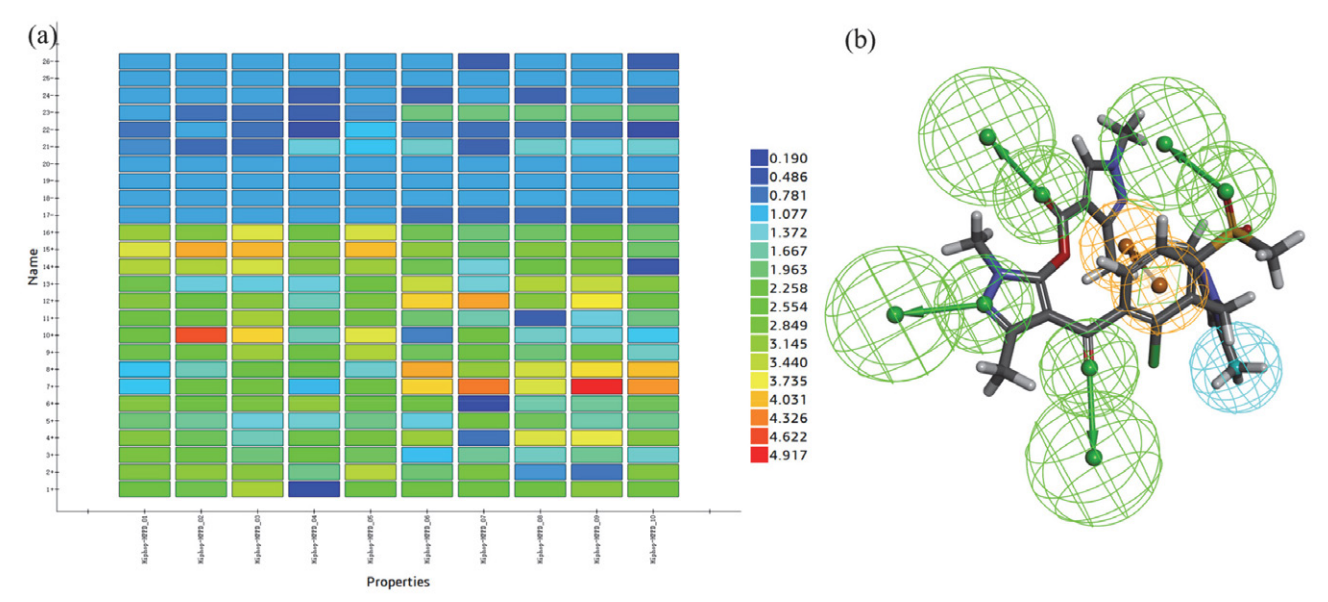


Figure 3. HPPD-Hiphop pharmacophore. (a) The heat map of the 10 hypotheses in the test; (b) The matching of pharmacophore model-02 with tripyrasulfone, the color of pharmacophore features RA, HY and HBA are represented by orange, blue and green, respectively. RA: The aromatic ring needs to be defined by two parameters: one parameter was the spatial position of the aromatic ring and the other parameter was the direction of the aromatic ring plane vector. HY: The hydrophobic center need not be represented by a vector. HBA: Hydrogen bond interaction has a clear directivity, and two points are used to describe hydrogen bond characteristics. One point represents the spatial position of the heavy atom in the hydrogen bond feature, and the other point represents the vector direction of the hydrogen bond acceptor.

Ten PPO pharmacophore models were generated ranking above 95 and had six characteristic elements, 2 aromatic ring centers, 2 hydrophobic characteristics and 2 hydrogen bond receptors, as shown in Table 2. The matching between the training set and the PPO-Hiohop pharmacophore models showed that the benzene ring in the compound produced the aromatic ring center, and the hydrogen bond receptor was formed nearby the oxygen atom. The hydrophobic features were observed between methyl and fluorine atom (Figure S6). Consistent with the test method of HPPD, according to the rank and the matching between the testing set and pharmacophore (Figure 4(a)), Hiphop pharmacophore model-01 was finally selected for subsequent screening, which included 2 aromatic ring centers, 2 hydrophobic features and 2 hydrogen bond receptors (Figure 4(b)).

Table 2 Result parameters of PPO-Hiphop pharmacophore model.

Num- ber	Features	Rank	Direct Hit	Partial Hit	Max Fit
01	RRHHAA	96.17	111111	000000	6
02	RRHHAA	96.17	111111	000000	6
03	RRHHAA	96.16	111111	000000	6
04	RRHHAA	96.16	111111	000000	6
05	RRHHAA	96.15	111111	000000	6
06	RRHHAA	96.12	111111	000000	6
07	RRHHAA	95.96	111111	000000	6
08	RRHHAA	95.96	111111	000000	6
09	RRHHAA	95.40	111111	000000	6
10	RRHHAA	95.40	111111	000000	6

Rank: Indicates the fit values of the pharmacophore.

Direct Hit: indicates the match between the pharmacophore and the training set molecule.

Partial Hit: indicates the number of pharmacophore features that match the training set molecule.

Max Fit: indicates the matching of pharmacophore features.

3. 2. CBP Pharmacophore for Virtual Screening

As for the PCA of compounds (Figure 5(a)), the data of active compounds and inactive compounds was distributed widely. There was a clear separation between the two groups, which could be used to validate the model. The ten generated HPPD pharmacophore models have more than five characteristic elements and the area under the curve (AUC) value was above 0.7, as shown in Table 3. According to the AUC value, the HPPD-CBP-01 model (AUC = 0.976) was selected for virtual screening. The HP-PD-CBP-01 contained aromatic ring centers, the hydrogen bond receptor and the hydrophobic group. Hydrogen bond acceptor was located at the oxygen atom, the six-membered ring center and the methyl group generated the hydrophobic feature (Figure 5(b)). The receiver operating characteristic curve (ROC) was used to verify the ability of the HPPD-CBP pharmacophore model to distinguish between active and inactive compounds, the accuracy of the CBP pharmacophore model was evaluated by AUC value, and ROC curves of ten CBP pharmacophore models were shown in Figure S7(a).

PCA was performed for PPO active compounds and inactive compounds, as shown in Figure 6(a), the spatial distribution of compounds was wide, active compounds and inactive compounds were distributed on two sides, with a clear demarcation line, the constructed model was verified by a test set. In ten PPO-CBP pharmacophore models, PPO-CBP-01 and PPO-CBP-02 included six characteristic elements, and the remaining models included five characteristic elements. According to the AUC values (Table 4), CBP pharmacophore models was selected for virtual screening. PPO-CBP-04 contained 2 hydrogen bond receptors, 2 hydrophobic features and 1 Harom (Figure 6(b)). Figure S7(b) shows the ROC of ten CBP pharmacophore models.

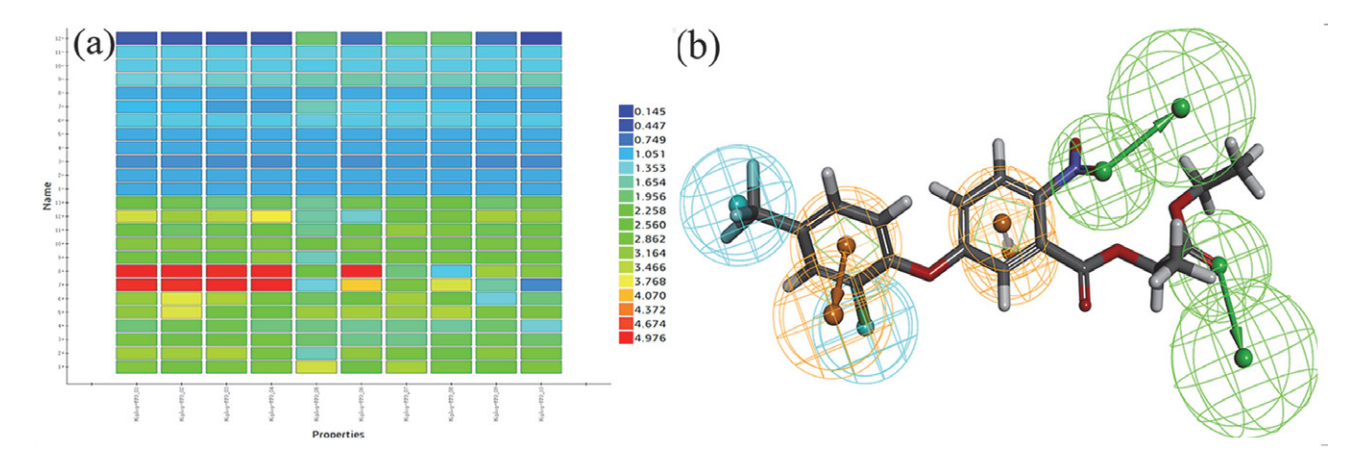


Figure 4. PPO-Hiphop pharmacophore. (a) The heat map of the 10 hypotheses in the test; (b) The matching of pharmacophore model-01 with lactofen, the color of pharmacophore features RA, HY and HBA are represented by orange, blue and green, respectively. RA: The aromatic ring needs to be defined by two parameters: one parameter was the spatial position of the aromatic ring and the other parameter was the direction of the aromatic ring plane vector. HY: The hydrophobic center need not be represented by a vector. HBA: Hydrogen bond interaction has a clear directivity, and two points are used to describe hydrogen bond characteristics. One point represents the spatial position of the heavy atom in the hydrogen bond feature, and the other point represents the vector direction of the hydrogen bond acceptor.

Table 3 Result parameters of HPPD-CBP pharmacophore model.

Numbe	r TP	TN	FP	FN	SE	SP	AUC	Features
01	45	68	1	2	0.96	0.98	0.98	AAHHRR
02	42	66	3	5	0.89	0.96	0.94	AAHHRR
03	45	68	1	2	0.96	0.98	0.98	AAHHRR
04	43	66	3	4	0.91	0.96	0.95	AAHHRR
05	47	52	17	0	1.00	0.75	0.91	AAHHHaromR
06	45	53	16	2	0.96	0.77	0.89	AAHHHaromR
07	47	53	16	0	1.00	0.77	0.89	AAHHHaromR
08	46	54	15	1	0.98	0.78	0.90	AAHHHaromR
09	32	59	10	15	0.68	0.86	0.75	DHHRR
10	32	59	10	15	0.68	0.86	0.75	DHHRR

TP: true positive; TN: true negative; FP: false positive; FN: false negative; SE: sensitivity; SP: specificity.

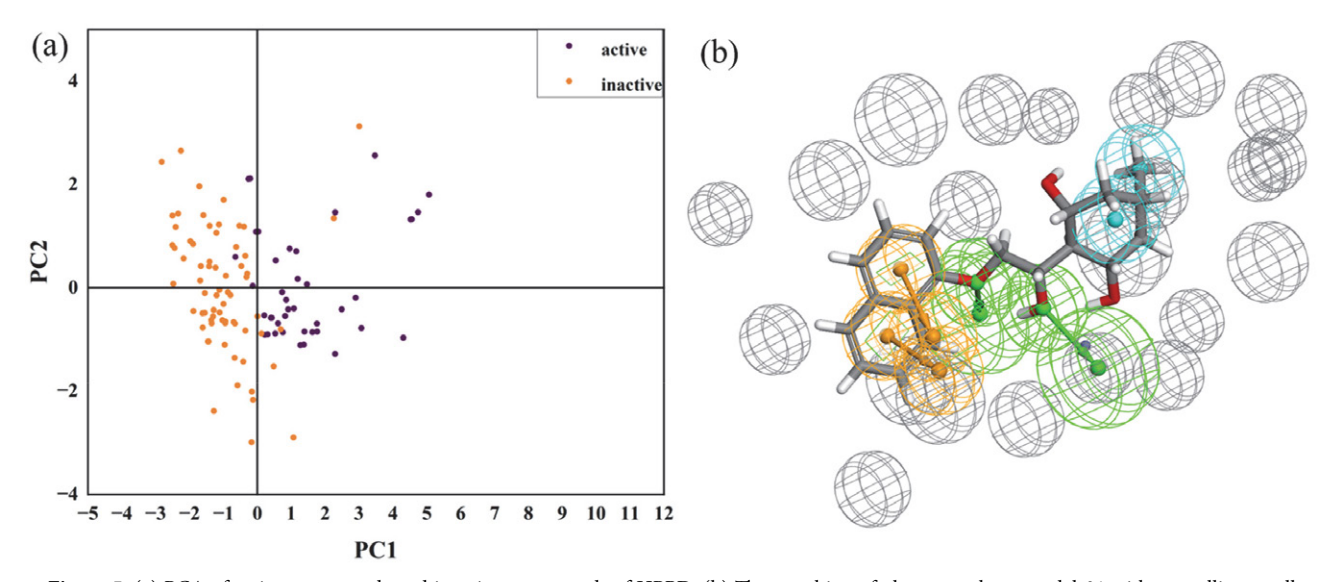


Figure 5. (a) PCA of active compounds and inactive compounds of HPPD; (b) The matching of pharmacophore model-01 with crystalline small compound.

Table 4 Result parameters of PPO-CBP pharmacophore model.

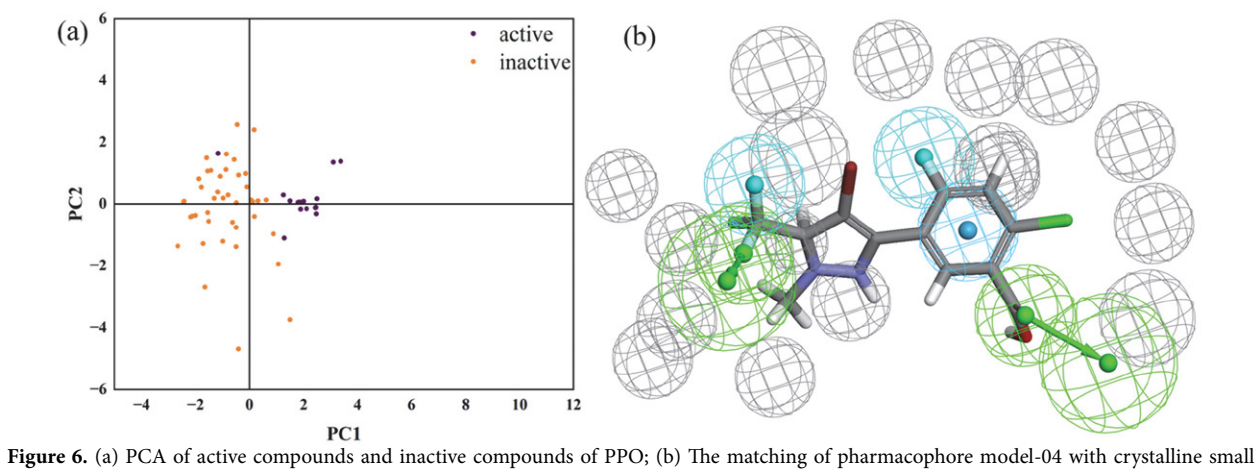
Number	TP	TN	FP	FN	SE	SP	AUC	Features
1	15	43	0	4	0.79	1.00	0.89	AAFFHalHarom
2	17	43	0	2	0.89	1.00	0.95	AAFFHalHarom
3	17	43	0	2	0.89	1.00	0.95	AAFFHal
4	18	43	0	1	0.95	1.00	0.97	AAFFHarom
5	18	42	1	1	0.95	0.98	0.97	AAFFHalHarom
6	18	42	1	1	0.96	0.98	0.97	AAFFHalHarom
7	17	43	0	2	0.89	1.00	0.95	AAFFHal
8	18	43	0	1	0.96	1.00	0.97	AAFFHarom
9	18	43	0	1	0.96	1.00	0.97	AAFFHalHarom
10	18	43	0	1	0.96	1.00	0.97	AAFFHalHarom

TP: true positive; TN: true negative; FP: false positive; FN: false negative; SE: sensitivity; SP: specificity

3. 3. Pharmacophore Virtual Screening

Before the virtual screening, the database was preprocessed. 1024513 Compounds, extracted from Bailingwei and Vitas-M databases, were screened according to the Lipinski principle: MW \leq 500, HBD < 5, HBA < 10, log p < 5, RB \leq 10. 498843 screened compounds were used to create a 3D database for the future investigations. HipHop pharmacophore model and CBP pharmacophore model were used to screen the compounds, and the intersection compounds of the two models were selected for further study.

83042 Compounds were screened through the Hiphop pharmacophore of HPPD-02, and the hit compounds were



compound.

 $\textbf{Table 5} \ \text{FitValues of compounds and pharmacophore model}.$

Name	Structure	FitValue ^a	FitValue ^b	FitValue ^c	FitValue ^d
Compound49317	F-(F-(N))	3.29	3.73	3.28	2.91
Compound10674	FOND	3.01	3.62	3.01	2.57
Compound35215	PHO N	3.11	3.36	2.89	2.50
Compound1555		3.15	3.49	3.47	2.12
STOCK1N-41398		3.15	3.1491	3.35	2.64
STOCK1N-67214	\$-0-6	3.06	3.69	3.18	2.64
STOCK1N-57851		3.19	3.25	2.52	2.58
STOCK1N-40313	O CI	3.59	3.36	3.55	2.51

a: Hiphop-HPPD FitValue; b: Hiphop-PPO FitValue; c: CBP-HPPD FitValue; d: CBP-FitValue

sent to the PPO-01 pharmacophore model, finally, 3571 compounds were obtained with the FitValue greater than 2. The CBP pharmacophore virtual screening was similar to Hiphop model. HPPD-01 was employed to screen 498843 compounds, 58300 compounds could hit the pharmacophore model, the hit compounds were filtered the PPO-04 model, 164 compounds were matched to the model. Finally, 8 cross-compounds were obtained by Hiphop model and CBP model, the FitValues were shown in Table 5.

ADMET properties play a crucial role in drug discovery for the druggability and safety. ADMET predic-

tions were performed to evaluate the solubility and safety profiles of the selected compounds. The DS "Calculate Molecular Properties" module under the "ADMET Descriptors" function was used for ADMET prediction, set evaluation option while maintaining default other Settings. The molecular properties (Table S4) and ADMET predictions (Table S5) of the selected compounds showed satisfactory results. It was evident from the predictions that all compounds exhibited good solubility. In addition, based on the CYP2D6 binding value, none of the 8 compounds showed inhibition CYP2D6, indicating their potential to avoid ab-

Table 6 The structure and evaluation of the potential compounds.

Compound	Structure	-CDOCKER ENERGY-HPPD (kcal/mol)	-CDOCKER ENERGY-PPO (kcal/mol)
Natural ligand		15.61	4.72
Negative compound	\(\sqrt{\sqrt{NH}}\)	5.49	3.84
Mesotrione		19.70	-
Oxyfluofen	HULL !	-	18.52
Compound49317		32.75	19.07
Compound10674		34.14	25.48
Compound35215		14.54	14.39
Compound1555	diana	36.73	25.58
STOCK1N-41398		24.87	24.15
STOCK1N-67214	\$	32.21	14.48
STOCK1N-57851	floh	34.61	34.81
STOCK1N-40313	OF HN OCI	43.74	36.63

normal blood concentration due to CYP2D6 inhibition. Additionally, the binding form and stability of these 8 compounds were conducted.

3. 4. Molecular Docking

To test the binding mode of the 8 hit compounds to the target, the CDOCKER program in DS was carried out, retenting the result of a high CDOCKER ENERGY value. Before the molecular docking, the natural ligand was redocked to protein to verify the reliability of the docking procedure, and the natural ligand was extracted for hydrogenation and energy minimization. As shown in Figure S8, the redocking ligand (brown) and the natural ligand (blue) almost completely overlapped, the RMSD values between HPPD, PPO and the natural ligand were 0.599 and 0.892, indicating that the CDOCKER procedure was reliable.

Eight compounds were docked with 1TFZ and 1SEZ, the results were analyzed according to the -CDOCKER ENERGY value. As shown in Table 6, for HPPD, the -CDOCKER ENERGY was higher than that the natural ligand except Compound35215. In PPO, the results of all

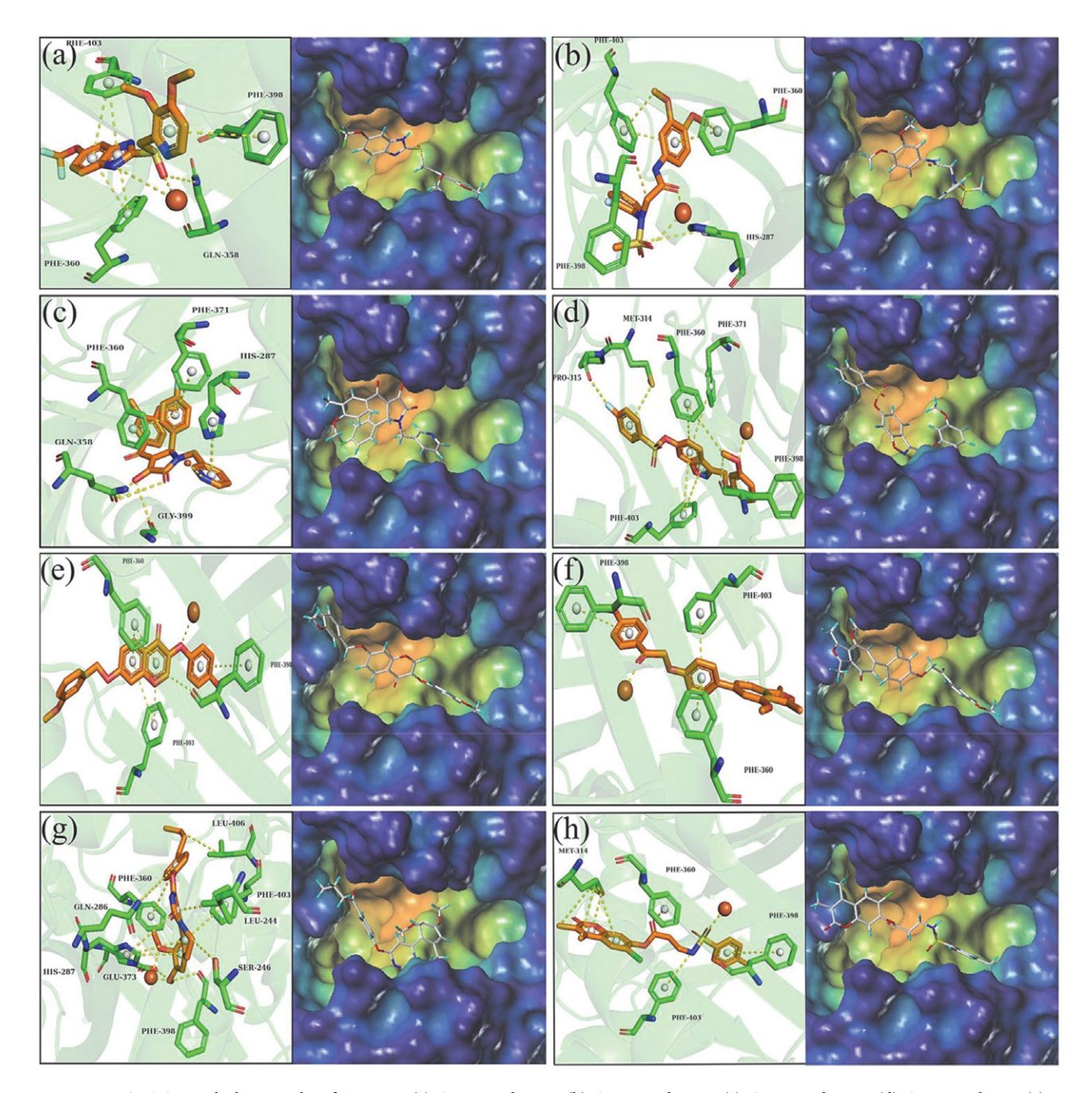


Figure 7. CDOCKER docking results of *At*HPPD. (a) Compound49317; (b) Compound10674; (c) Compound35215; (d) Compound1555; (e) STOCK1N-41398; (f) STOCK1N-67214; (g) STOCK1N-57851; (h) STOCK1N-40313 interact with receptor-ligand at the active site of *At*HPPD.

compounds were superior to the natural ligand. The commercial herbicides mesotrione and oxyfluofen were selected for molecular docking with *At*HPPD and *Nt*PPO, and it was found that except Compound35215, the –CDOCK-ER_ENERGY of the other 7 compounds were superior to the commercial herbicides. The docking results of negative compound showed that all compounds had good docking results, which were higher than negative compound.

The interactions between HPPD and ligands were shown in Figure 7. All the 8 compounds could chelate with the metal Fe(II). Compound49317, Compound10674, and

STOCK1N-57851 formed bidentate combination. The hot spot residues Phe403 and Phe360 binded to the benzene ring via π - π interaction. Phe398 binded to ligands in two ways, one was the π - π interaction with the aromatic rings of Compound49317, STOCK1N-41398, STOCK1N-67214 and STOCK1N-40313, another way of binding was to hydrogen bond interactions with the hydrogen atoms of Compound10674, Compound1555, STOCK1N-41398, STOCK1N-57851, and STOCK1N-40313. In addition to a metal ligand, Phe403, Phe398, and Phe360, the formation of interactions between ligands and other residues (His287,

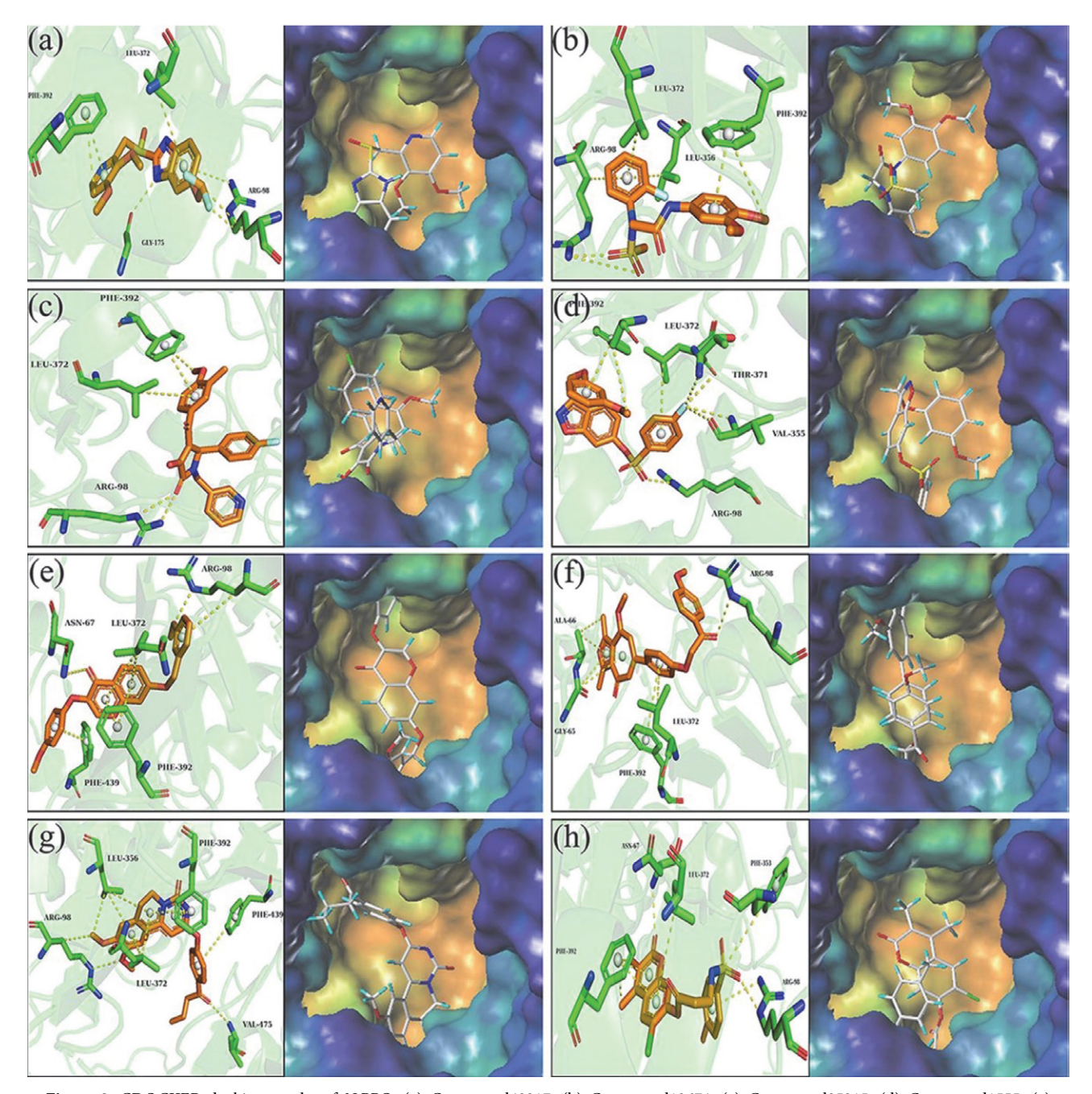


Figure 8. CDOCKER docking results of *Nt*PPO. (a) Compound49317; (b) Compound10674; (c) Compound35215; (d) Compound1555; (e) STOCK1N-41398; (f) STOCK1N-67214; (g) STOCK1N-57851; (h) STOCK1N-40313 interact with receptor-ligand at the active site of *Nt*PPO.

Phe360, Phe371, Met314) was also beneficial to improve the binding stability of the compound to the target, which enhanced the inhibition effect.

The interactions between PPO and ligands were shown in Figure 8. There were hydrogen bond interactions with Arg98 and oxygen atoms in 8 ligands, and π - π interactions with Phe392 and aromatic rings, all ligands produced π -alkyl interactions with Leu372. The π - π interacobserved in STOCK1N-41398 tion STOCK1N-57851 with Phe439, and the π -alkyl interaction was identified in Compound10674, Compound35215, STOCK1N-67214 and STOCK1N-40313 with Phe439. By molecular docking analysis with AtHPPD and NtPPO, it was found that all compounds could bind to the key residues of two targets, and obtained similar docking scores with commercial herbicides.

3. 4. MD Simulation

The MD simulation was employed to verify the stability of the binding of the compound to the protein. The simulation time was set at 100 ns, and a stable system was obtained. The results were expressed using the root-mean-square deviation (RMSD), which included the $C\alpha$ atom of the protein backbone, the heavy atom of the ligand, and the active pocket of the residues around the ligand. As shown in Figure 9(a)(b)(c), in the process of binding with HPPD, Compound35215 fluctuated at the first 10 ns and stabilized after 20 ns. Compound49317, Compound10674 and STOCKIN-57851 did not fluctuate significantly after

15 ns. Compared with the natural ligand in 1TFZ, the RMSD of STOCKIN-40313, STOCKIN-41398 and Compound35215 were similar as the native ligand. The RMSD values for Compound10674, Compound35215, Compound49317, STOCKIN-57851, and STOCKIN-67214 were comparable to those of commercial herbicides. In contrast, the RMSD values for Compound1555, Compound40313, and Compound41398 were lower than those observed for mesotrione. 8 Compounds maintained good stability during MD simulation. As shown in Figure 9(d) (e)(f), STOCKIN-57851, STOCKIN-41398 and STOCK-IN-40313 kept stable after 15 ns with the PPO protein. 3 Compounds showed lower RMSD than natural ligand. Compound10674 and STOCKIN-67214 began to level off after 40 ns. Exception of Compound 35215, the RMSD values for the other seven compounds were comparable to those of the commercial herbicide oxyfluofen. All compounds tended to stabilize after a certain period of time, which proved that the screened compounds could stably bind to the target. In HPPD and PPO targets, the screened compounds showed good stability in MD simulation, which further indicated that the screened compounds could form stable structures with the targets.

As shown in Figure S9, the residues Phe403, Glu373, Phe398, His287, Phe360 and His205 in HPPD contributed significantly to the protein binding process of the natural ligand, Compound49317, Compound10674 and STOCK-IN-57851. Similar to HPPD analysis, in the binding process of PPO to ligand, Phe392, Leu372, Leu356 and Arg98 contributed greatly, these residues were the key residues of

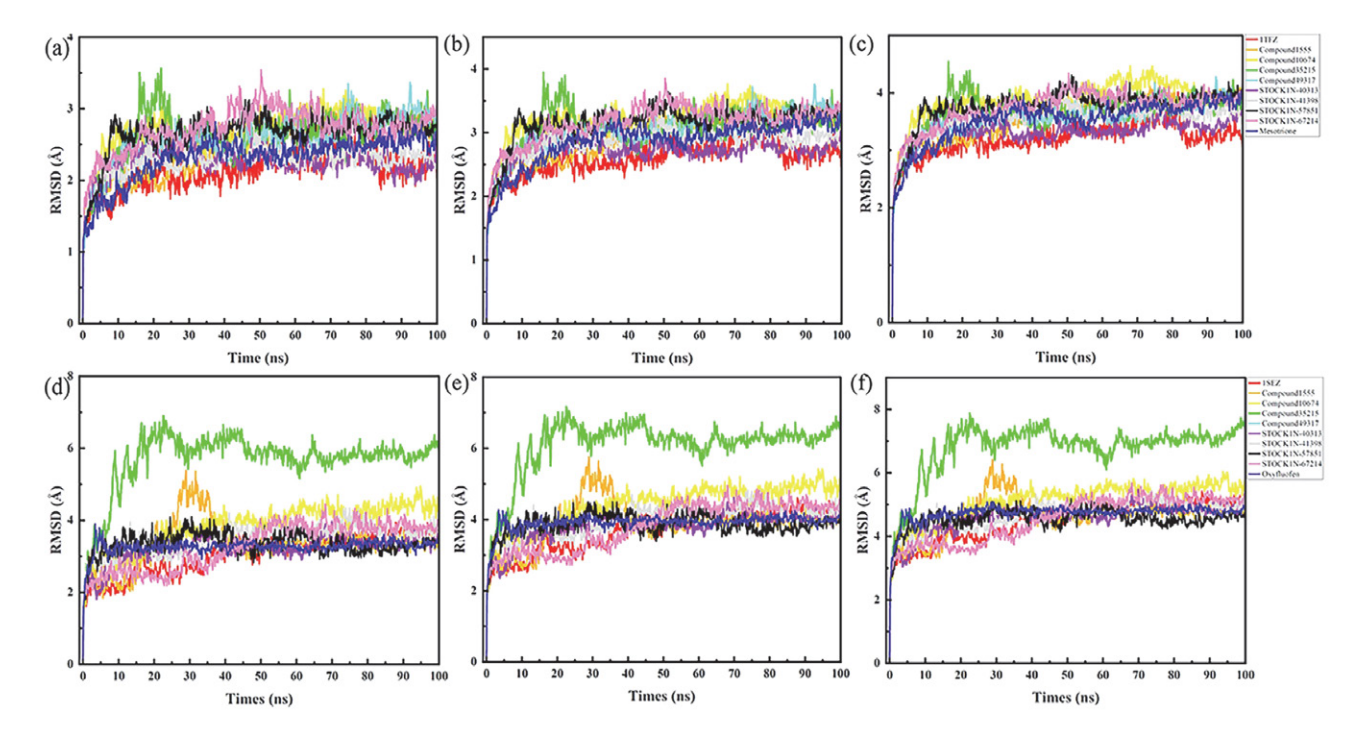


Figure 9 (a) AtHPPD-RMSD of skeleton $C\alpha$ atom; (b) AtHPPD-RMSD of the heavy atom of the ligand; (c) AtHPPD-RMSD of the protein active pocket with 5 Å residues around the ligand. (e) NtPPO-RMSD of skeleton $C\alpha$ atom; (f) RMSD of the heavy atom of the ligand; (g) RMSD of the protein active pocket with 5 Å residues around the ligand.

PPO protein. In addition to key residues, Thr68 and Phe439 also played key roles in MD simulation.

The acceptor-ligand binding free energy (ΔG_{bind}) was calculated using the MM/GBSA method. Table 7 gave the parameters of ΔG_{bind} , ΔG_{bind} coulomb, ΔG_{bind} Hbond, $\Delta Gbind\ Lipo\ and\ \Delta G_{bind}\ vdW$. The $\Delta G_{bind}\ value\ reflected$ the degree of binding between the compound and HPPD. Among the 8 compounds, ΔG_{bind} Covalent was positive values, indicating that ΔG_{bind} Covalent formed negative effect on protein binding, and the calculated values of ΔG_{bind} Lipo and $\Delta G_{bind} vdW$ were both negative, according to the parameters, it was concluded that ΔG_{bind} Lipo and ΔG_{bind} vdW were the main contributors of binding free energy. The ΔG_{bind} values of STOCK1N-57851, STOCK1N-40313 and STOCK1N-67214 were -41.03 kcal mol⁻¹, -26.14 kcal mol⁻¹ and -24.75 kcal mol⁻¹, respectively. STOCK1N-57851 showed the greatest binding force with the protein. ΔG_{bind} Coulomb was -38.37 kcal mol⁻¹, ΔG_{bind} Hbond was -0.75kcal mol⁻¹ and ΔG_{bind} Lipo was -24.87 kcal mol⁻¹, ΔG_{bind} vdW was -48.05 kcal mol⁻¹. According to the residue contribution degree and binding free energy, the compound had the potential to be an inhibitor of HPPD.

As shown in Table 8, similar as the HPPD complex, most of the ΔG_{bind} Covalent in 8 compounds were mostly positive, which had a negative effect on protein binding G_{bind} Lipo and ΔG_{bind} vdW were major contributors to binding free energy. The ΔG_{bind} values of STOCK1N-57851, STOCK1N-40313 and STOCK1N-41398 were -73.20 kcal mol⁻¹, -52.53 kcal mol⁻¹ and -57.40 kcal mol⁻¹, respectively. The ΔG_{bind} vdW of STOCK1N-57851 and STOCK1N-40313 were -48.05 kcal mol⁻¹ and -46.54 kcal

mol⁻¹, respectively. The results confirmed that STOCK1N-57851 had good binding ability for both HP-PD and PPO.

4. Conclusion

In summary, based on commercial inhibitors and crystalline complexes of two herbicide targets enzyme (HPPD and PPO), Hiphop pharmacophore and CBP pharmacophore models were constructed for screening, respectively. Eight potential molecules were obtained for further molecular docking, ADMET prediction, dynamics studies and binding free energy calculation. All the eight compounds matched with AtHPPD and NtPPO well. The selected ligands were in line with drug formation and had the advantages of low toxicity and no pollution, which were in accord with the current concept of developing green pesticides and had the potential to become double target herbicides. STOCK1N-57851 interacted with the key residues Arg98, Phe392, Leu372 and Phe439 in PPO active site, blocking the synthesis of chlorophyll. For HPPD receptor, in addition to interacting with the key residues, it also formed bidentate combination with Fe(II), by occupying the active site. This compound prevented HP-PD from participating in the biosynthesis of plastoquinone and tocopherol in plants, thereby inhibiting photosynthesis. In general, STOCK1N-57851 was regarded as a promising potential dual-target inhibitor of HPPD and PPO, providing valuable insights for the design of novel molecular frameworks.

Table 7 HPPD-Contribution of various energy components to binding free energy (kcal mol⁻¹).

Compound	ΔG_{bind}	ΔG_{bind} Coulomb	ΔG_{bind} Covalent	$\Delta G_{bind} H_{bond}$	ΔG_{bind} Lipo	$\Delta G_{bind} vdW$
STOCK1N-57851	-41.03	-38.37	8.82	-0.75	-24.87	-48.05
Compound35215	-19.21	-9.06	9.32	-0.68	-24.62	-44.61
Compound49317	-6.13	-25.56	1.18	-0.04	-15.09	-49.95
Compound10674	-18.48	-49.48	7.58	0.06	-18.40	-41.38
STOCK1N-40313	-26.14	-18.88	8.60	0.015	-23.12	-46.54
STOCK1N-41398	-13.17	-38.47	11.75	-1.21	-21.46	-40.97
Compound1555	-14.74	-24.75	4.95	-0.04	-22.91	-45.11
STOCK1N-67214	-24.75	-46.54	9.074	-1.64	-23.89	-45.37

Table 8 PPO-Contribution of various energy components to binding free energy (kcal mol⁻¹).

Compound	ΔG_{bind}	ΔG_{bind} Coulomb	ΔG_{bind} Covalent	$\Delta G_{bind} H_{bond}$	ΔG _{bind} Lipo	$\Delta G_{bind} v dW$
STOCK1N-57851	-73.20	-9.00	6.64	-1.09	-28.73	-55.94
Compound35215	-62.33	-19.49	-1.63	-1.62	-20.46	-46.59
Compound49317	-64.99	10.45	3.92	-0.62	-14.752	-56.75
Compound10674	-46.15	-12.52	2.96	-2.11	-10.45	-44.71
STOCK1N-40313	-52.53	-0.477	10.04	-1.09	-18.77	-54.96
STOCK1N-41398	-57.40	-12.99	6.15	-0.99	-21.82	-49.68
Compound1555	-57.64	-12.06	1.58	-2.19	-19.085	-49.53
STOCK1N-67214	-64.28	-8.26	8.64	-0.02	-25.80	-60.66

Acknowledgment

This work was supported by the National Nature Science Foundation of China (No. 22077014, No. 32372589, No. 32311530764) and Natural Science Foundation of Heilongjiang Province (ZD2022C003). The authors are grateful to Prof. Jian Wang (Shenyang Pharmaceutical University) for helping in the application of SYBYL and Schrödinger software.

6. References

- Y. Fu, T. Ye, Y. X. Liu, J. Wang, F. Ye, Int. J. Mol. Sci. 2020, 21, 5546. DOI:10.3390/ijms21155546
- X. Y. Leng, S. Gao, Y. F. Ma, L. X. Zhao, M. Wang, F. Ye, Y. Fu, Pestic. Biochem Physiol. 2023, 192, 105390.
 DOI:10.1016/j.pestbp.2023.105390
- 3. P. E. Hulme, *Field. Crops. Res.* **2023**, *292*, 108819. **DOI**:10.1016/j.fcr.2023.108819
- Y. Fu, M. Wang, L. X. Zhao, S. Q. Zhang, Y. X. Liu, Y. Y. Guo,
 D. Zhang, S. Gao, F. Ye, *Pestic. Biochem. And. Physiol* 1. 2021,
 74, 104811.
- J. Shi, H. F. Cao, C. F. Wang, S. Gao, J. Y. Wang, L. X. Zhao, F. Ye, Y. Fu, J. Taiwan. Inst. Chem. Eng. 2023, 143, 104711.
 DOI:10.1016/j.jtice.2023.104711
- E. A. Borgato, A. Thiagarayaselvam, D. E. Peterson, M. M. Hay, J. A. Dille, M. Jugulam, J. Agric. Food. Chem. 2024, 72, 5122–5132. DOI:10.1021/acs.jafc.3c05333
- B. F. Zheng, Y. Zuo, G. Y. Huang, Z. Z. Wang, J. Y. Ma, Q. Y. Wu, G. F. Yang, *J. Agric. Food. Chem.* 2023, 21, 14221–14231.
 DOI:10.1021/acs.jafc.3c03593
- W. Zhang, J. H. Zhang, C. H. Yan, X. H. Gan, J. Agric. Food. Chem. 2024, 72, 12946–12955.
 DOI:10.1021/acs.jafc.4c00272
- W. Geng, Q. Zhang, L. Liu, G.Y. Tai, X. H. Gan, *J. Agric. Food. Chem.* 2024, 72, 17191–17199.
 DOI:10.1021/acs.jafc.4c01389
- 10. N. Alnafta, R. Beffa, G. Bojack, B. Bollenbach-Wahl, N. Z. Brant, C. Dörnbrack, N. J. Dorn, Freigang, E. Gatzweiler, R. Getachew, C. Hartfiel, I. Heinemann, H. Helmke, S. Hohmann, H. Jakobi, G. Lange, P. Lümmen, L. Willms, J. Frackenpohl, J. Agric. Food. Chem. 2023, 71, 18270–18284. DOI:10.1021/acs.jafc.3c01420
- D. W. Wang, H. Zhang, S. Y. Yu, R. B. Zhang, L. Liang, X. Wang, H. Z. Yang, Z. Xi, J. Agric. Food Chem. 2021, 69, 14115–14125. DOI:10.1021/acs.jafc.1c05665
- H.Y. Liu, L. K. Yu, S. N. Qin, H. Z. Yang, D. W. Wang, Z. Xi, J. Agric. Food. Chem. 2023, 71, 3225–3238.
 DOI:10.1021/acs.jafc.2c09082
- 13. E. Ivantsova, I. Konig, V. Lopez-Scarim, C. English, S. R. Charnas, C. L. Souders, C. J. Martyniuk, *Environ. Toxicol. Pharmacol.* **2023**, *98*, 104084. **DOI:**10.1016/j.etap.2023.104084
- 14. H. Lu, Q. Yu, H. Han, M. J. Owen, S. B. Powles, *Pest. Manag. Sci.* **2020**, *76*, 2015–2020. **DOI:**10.1002/ps.5733
- L. Yang, D. Wang, D. Ma, D. Zhang, N. Zhou, J. Wang, H. Xu,
 Xi, Molecules. 2021, 26, 6979.

- **DOI:**10.3390/molecules26226979
- C. Chen, Q. Lei, W. Geng, D. Wang, X. Gan, Food. Chem.
 2024, 72, 12425–12433. DOI:10.1021/acs.jafc.3c09350
- R. Dreesen, A. Capt, R. Oberdoerfer, I. Coats, K.E. Pallett, Regul. Toxicol. Pharm. 2018, 97, 170–185.
 DOI:10.1016/j.yrtph.2018.06.002
- X. L. Sun, Z. M. Ji, S. P. Wei, Z. Q. Ji, J. Agric. Food. Chem. 2020, 68, 15107–15114.
- J. Dong, J. Q. Dong, X. H. Yu, Y. C. Yan, J. X. Nan, B. Q. Ye,
 W.C. Yang, H. Y. Lin, G. F. Yang, J. Agric. Food. Chem. 2023,
 71, 1170–1177. DOI:10.1021/acs.jafc.2c06727
- Z. B. Jiang, S. Gao, W. Hu, B. R. Sheng, J. Shi, F. Ye, Y. Fu, Design, *Pestic. Biochem. Physiol.* 2023, 194, 105493.
 DOI:10.1016/j.pestbp.2023.105493
- H. Y. Lin, J. Dong, J. Dong, W. C. Yang, G. F. Yang, Trends. Biochem. Sci. 2023, 48, 568–584.
 DOI:10.1016/j.tibs.2023.02.006
- X. Gong, G. Zhao, W. Shan, H. Guo, C. Wang, Q. Liu, B. Xu,
 Y. Wang, X. Guo, *Pestic. Biochem. Physiol.* 2022, 184, 105110.
 DOI:10.1016/j.pestbp.2022.105110
- J. P. Sun, J. W. Zan, X. N. Zang, Int. J. Mol. Sci. 2022, 23, 3122.
 DOI:10.3390/ijms23063122
- M. Zhang, H. Cai, D. Ling, C. Pang, J. Chang, Z. Jin, Y. R. Chi, J. Agric. Food. Chem. 2023, 71, 16972–16983.
- W. Zhang, J. Pei, L. Lai, J. Chem. Inf. Model. 2017, 57, 403–412.
 DOI:10.1021/acs.jcim.6b00491
- T. Wei, R. Lin, X. Fu, Y Lu, W. Zhang, Z. Li, J. Zhang, H. Wang, *Pharmacol. Res.* 2022, 180, 106244.
 DOI:10.1016/j.phrs.2022.106244
- S. C. Yen, L. C. Chen, H. L. Huang, W. C. Huangfu, Y. Y. Chen,
 T. Eight Lin, S. T. Lien, H. J. Tseng, T. Y. Sung, J. H. Hsieh, W.
 J. Huang, S. L. Pan, K. C. Hsu, *Bioorg. Chem.* 2022, *21*, 105675.
- S. Liu, H. H. Qin, X. R. Ji, J. W. Gan, M. J. Sun, J. Tao, Z. Q. Tao, G. N. Zhao, B. X. Ma, J. Agric. Food. Chem. 2023, 71, 8038–8049. DOI:10.1021/acs.jafc.3c00867
- M. Koch, C. Breithaupt, R. Kiefersauer, J. Freigang, R. Huber,
 A. Messerschmidt, *EMBO. J.* **2004**, *23*, 1720–1728.
 DOI:10.1038/sj.emboj.7600189
- C. Yang, J. W. Pflugrath, D. L. Camper, M. L. Foster, D. J. Pernich, T. A. Walsh, *Biochemistry*. 2004, 43, 10414–10423.
 DOI:10.1021/bi0493230
- A. Ilic, N. Djokovic, T. Djikic, K. Nikolic, Comput. Biol. Chem. 2024, 113, 108242.
 - DOI:10.1016/j.compbiolchem.2024.108242
- T. Zhang, Y. Hua, C. Zhou, Y. Xiong, D. Pan, Z. Liu, Y. Dang, Food. Chem. 2022, 394, 133504.
 DOI:10.1016/j.foodchem.2022.133504
- 33. Y. X. Liu, S. Gao, T. Ye, J. Z. Li, F. Ye, Y. Fu, Future. Med. Chem. **2020**, *12*, 795–811. **DOI:**10.4155/fmc-2019-0349
- 34. Y. Sun, Y. Jiao, C. Shi, Y. Zhang, *Biotechnol. J.* **2022**, *20*, 5014–5027. **DOI**:10.1016/j.csbj.2022.09.002
- 35. S. Rajasekhar, S. Das, R. Karuppasamy, M. B. Musuvathi, K. Chanda, *J Comput. Chem.* **2022**, *43*, 619–630. **DOI:**10.1002/jcc.26823
- 36. S. Rajasekhar, R. Karuppasamy, K. Chanda, *J. Comput. Chem.* **2021**, *42*, 1736–1749. **DOI:**10.1002/jcc.26712

- 37. G. Borhan, M. Sahihi, *J. Mol. Model.* **2024**, *133*, 108882. **DOI:**10.1016/j.jmgm.2024.108882
- I. Kucuk, Ö. B. Küçükşahin, M. Yildirim, M. Z. Kabir, H. Silah, I. Celik, *Spectrochim. Acta. A.* 2024, 326, 125246.
 DOI:10.1016/j.saa.2024.125246
- X. Li, Y. J. Liu, B. B. Nian, X. Y. Cao, C. P. Tan, Y.F. Liu, Y. J. Xu, Food. Chem. 2022, 373, 131285.
 DOI:10.1016/j.foodchem.2021.131285
- Y. Wang, L. X. Zhao, J. Shi, S. Gao, F. Ye, Y. Fu, J. Mol. Liq. 2022, 362, 119683. DOI:10.1016/j.molliq.2022.119683
- J. Shi, L.X. Zhao, J. Y. Wang, T. Ye, M. Wang, S. Gao, F. Ye, Y. Fu, *Arab. J. Chem.* 2022, *15*, 103919.
 DOI:10.1016/j.arabjc.2022.103919
- G. Poli, C. Granchi, F. Rizzolio, T. Tuccinardi, *Molecules*.
 2020, 25, 1971. DOI:10.3390/molecules25081971

Povzetek

Razvoj in identifikacija herbicidov z dvojno tarčo je eden izmed glavnih pristopov za reševanje problema odpornosti plevela. Protoporfirinogen oksidaza (PPO) in p-hidroksifenilpiruvat dioksigenaza (HPPD) sta dve pomembni tarči v fotosintezi rastlin. V nasprotju s tradicionalnim načrtovanjem zdravil, ki temeljijo na eni sami tarči, se ta študija osredotoča na oblikovanje zdravil z dvojnim učinkom na HPPD in PPO. Hiphop farmakoforni modeli za tarči HPPD in PPO so bili izdelani z uporabo komercialnih pesticidov, farmakoforni modeli CBP pa so bili napravljeni na podlagi proteinskih kompleksov. Z uporabo farmakofornih modelov smo pregledali več milijonov molekul, izmed katerih smo jih izbrali 8. Kandidatne spojine so tvorile kelate z železom (Fe II) v HPPD in vypostavile stabilne π - π interakcije s ključnimi ostanki v aktivnem mestu HPPD. Večina spojin je tvorila vodikove vezi in π - π interakcije z ostanki v PPO. V kombinaciji z večstopenjskim vizualnim presejalnim postopkom smo pridobili potencialne spojine z zaviralnim učinkom na obe tarči.



Except when otherwise noted, articles in this journal are published under the terms and conditions of the Creative Commons Attribution 4.0 International License